Methanol mediated direct CO<inf>2</inf> hydrogenation to hydrocarbons: Experimental and kinetic modeling study

Chemical Engineering Journal 435 (2022) 135090

Contents lists available at ScienceDirect

Chemical Engineering Journal

journal homepage: www.elsevier.com/locate/cej

Methanol mediated direct CO_2 hydrogenation to hydrocarbons: Experimental and kinetic modeling study

Sreetama Ghosh, Louise Olsson, Derek Creaser *

Chemical Engineering, Competence Centre for Catalysis, Chalmers University of Technology, SE – 41296 Gothenburg, Sweden

ARTICLE INFO

Keywords:
Carbon capture and utilization (CCU)
CO_2 hydrogenation to hydrocarbon
Bifunctional catalytic bed
Kinetic model

ABSTRACT

Carbon dioxide can be utilized as a feedstock to produce chemicals and renewable fuels sustainably. CO_2 hydrogenation to hydrocarbons through a methanol mediated pathway requires a more detailed study, examining interactions between reaction processes leading to different product selectivities. In this particular work, we propose a kinetic model for the direct CO_2 hydrogenation to different hydrocarbon products over an In_2O_3/HZSM-5 bifunctional catalytic bed. The model includes a CO_2 hydrogenation to methanol model based on a Langmuir Hinshelwood Hougen Watson (LHHW) reaction mechanism over In_2O_3 catalyst combined with a *lump*-type methanol to hydrocarbon (MTH) model over the HZSM-5 zeolite. Interestingly, the combined model could largely predict the suppression of the reverse water gas shift (RWGS) reaction and an increase in the yield of hydrocarbons compared to the formation of methanol in case of the same reaction conditions carried out with only the methanol synthesis catalyst (In_2O_3). Further, by varying the mass ratio of the individual components of the bifunctional catalytic bed, it was demonstrated that a higher outlet concentration of methanol achieved with a higher mass ratio of the methanol synthesis catalyst caused less suppression of the RWGS reaction and shifted the hydrocarbon product distribution to a slightly larger share of higher hydrocarbons. These changes in product selectivity caused by variation of the catalyst mass ratio were both also successfully reproduced by the model. Therefore, a comparison between the experimental results and the model predictions shows that this model, including equilibrium effects for the reactions, can accurately predict the trends of the experimental findings for direct CO_2 hydrogenation to hydrocarbons over the In_2O_3/HZSM-5 catalyst.

1. Introduction

The increase in anthropogenic carbon dioxide (CO_2) emissions due to the increasing utilization of fossil fuels have led to an enhancement in the global temperature causing global warming. It has a direct negative impact on the environment. The current total global anthropogenic CO_2 emission was about 31.5 Gt_{CO2} in 2020 according to the International Energy Agency (IEA). Consequently, carbon capture, storage and utilization have attracted attention in recent years to combat the negative effects of this greenhouse gas. The catalytic hydrogenation of CO_2 can be a green and climate-neutral process that can convert CO_2 directly to value-added chemicals like carbon monoxide (CO), methane (CH_4), methanol (CH_3OH), light olefins (C_2-$C_4^=$), liquified petroleum gas (C_3-C_4^0), gasoline (C_5-C_{11} hydrocarbons), etc. utilizing hydrogen produced from water electrolysis with renewable and sustainable energy sources [1–3]. Specifically, the growing demand for liquid fuels (C_5^+) and the gradual depletion of fossil fuel resources call for the urgent need for their production from renewable resources. But this is very challenging since CO_2 is an inert and thermodynamically stable molecule [4].

The CO_2 hydrogenation to hydrocarbon reaction can follow two alternative pathways: a) the modified Fischer-Tropsch synthesis (MFTS) and b) the methanol-mediated synthesis. In MFTS, CO_2 is firstly reduced to CO through the reverse water gas shift (RWGS) reaction and thereby CO is hydrogenated via an FTS process to form hydrocarbons. On the other hand, for the methanol-mediated alternative, CO_2 is first hydrogenated to methanol and then through the hydrocarbon pool mechanism, it is converted into hydrocarbons. The methanol-mediated process occurs in a single reactor and is potentially more energy-efficient and economical [5–6]. It is carried out over a bifunctional catalytic bed that enables the following two main reactions:

$$CO_2 + 3H_2 \rightleftharpoons CH_3OH + H_2O \quad (1)$$

$$2nCH_3OH \xrightarrow{-nH_2O} nCH_3OCH_3 \xrightarrow{-nH_2O} C_{2n}H_{4n} \quad (2)$$

* Corresponding author.
E-mail address: derek.creaser@chalmers.se (D. Creaser).

https://doi.org/10.1016/j.cej.2022.135090
Received 21 October 2021; Received in revised form 14 January 2022; Accepted 2 February 2022
Available online 5 February 2022

CO_2 hydrogenation to methanol is an exothermic reaction that occurs in parallel with the RWGS reaction, which is an endothermic reaction forming CO, favored at higher reaction temperatures. Methanol further is converted to olefins over acidic catalysts, mainly zeolites like ZSM-5 and SAPO-34, that are industrially used catalysts for methanol to olefin (MTO) reactions [6]. MTO is favorable at a temperature range of about 400–450 ℃ due to its kinetics with zeolite catalysts [7–8]. On the other hand, methanol can be produced from synthesis gas over Cu/ZnO/Al_2O_3 catalysts within a temperature range of 200–320 °C and pressure between 50 and 100 bar [9]. This is mainly because higher temperature favors the RWGS reaction and produces more CO that reduces the selectivity for methanol [10]. So, the amalgamation of both these processes (CO_2 to methanol + MTO) over the bifunctional catalytic bed necessitates a compromise in temperature, where too much CO formation can be avoided and the zeolite can also be sufficiently active for the C–C coupling [6].

Both In_2O_3 and HZSM-5 have received great attention as catalysts for methanol synthesis from CO_2 and methanol to gasoline (MTG) reactions respectively [1,11]. DFT calculations suggest that the oxygen vacancy sites for In_2O_3 act as the active sites for the synthesis of methanol directly from CO_2 via the formate pathway [12–13]. Further, the CH_3OH formed over the In_2O_3 catalyst transfers to the HZSM-5 zeolite which has strong acidic sites and large channels that help in forming long-chain hydrocarbons and aromatics via the hydrocarbon pool mechanism [1]. Dahl and Kolboe suggested the hydrocarbon pool mechanism where methanol forms a pool of $(CH_2)_n$ species inside the pores of the zeolite which further produce alkanes, light olefins and aromatics [14–15]. Later, the dual cycle concept introduced by Olsbye et al. suggested that olefinic and aromatic cycles run simultaneously during the methanol to hydrocarbon (MTH) reaction over HZSM-5 catalysts [16–17]. The six major steps for hydrocarbon formation from methanol in the dual cycle mechanism are hydrogen transfer, olefin cracking, olefin methylation, cyclization, aromatic dealkylation and aromatic methylation [18]. Apart from these, a similar kind of methanol mediated single step conversion of syngas to gasoline has been reported by Dagle et al. where they have mixed Pd/ZnO/Al_2O_3 and ZSM-5 to produce liquid hydrocarbons rich in aromatics [19].

Kinetic modeling studies can provide insights into reaction schemes and mechanisms. Kinetic models are reported for CO_2 hydrogenation to methanol [6,20–22]. Kinetics of low pressure methanol synthesis was studied by Graaf et al [23] where they have developed a dual-site Langmuir-Hinshelwood kinetic model and validated the model with experimental results over Cu-Zn-Al catalyst. Frei et al. described the mechanism and kinetics of CO_2 hydrogenation over an In_2O_3 catalyst using a microkinetic model [22]. Moreover, several kinetic studies are reported for the methanol to olefin process over HZSM-5 catalysts [6,24–25]. Park et al. formulated a detailed kinetic model for the MTO reaction over HZSM-5 catalyst where the surface oxonium ylide mechanism could explain the formation of the primary olefin and the carbenium ion mechanism the production of higher olefins [26]. A microkinetic model was developed by Kumar et al. [27] to demonstrate MTO reaction kinetics over HZSM-5 catalyst where they showed that dimethyl ether (DME) and primary olefins form through the aromatic hydrocarbon pool and higher olefins form via the alkene homologation cycle. A kinetic model with seven lumps was established by Aguayo et al. [28] which helps in the quantification of all the products formed at high temperatures (400–500 ℃) over an HZSM-5 catalyst for the methanol to hydrocarbon conversion reaction. Another model based on the hydrocarbon pool mechanism was proposed by Kaarsholm et al. in which olefins are generated via reversible reactions over a phosphorus modified ZSM-5 catalyst [29].

In our previous work, we have developed a kinetic model for CO_2 hydrogenation to methanol over an In_2O_3 catalyst based on a Langmuir Hinshelwood Hougen Watson (LHHW) reaction mechanism where we presented a kinetic model interpreting how the CO_2 hydrogenation to methanol and the RWGS reactions are coupled kinetically and thermodynamically by deriving a set of optimized kinetic parameters [21]. In the present work, we have extended the methanol model to develop a new kinetic model for the direct CO_2 hydrogenation to hydrocarbon by adding an MTH model to the existing methanol synthesis model. A lumped type kinetic model developed by Pérez-Uriarte et al. [30] for the reaction of dimethyl ether (DME) to olefins over HZSM-5 zeolite has been modified and used as the methanol to hydrocarbon (MTH) model in this work. To the best of our knowledge, no reports on kinetic models for direct CO_2 hydrogenation to hydrocarbons have yet been reported. And that brings the novelty of the current work, where we demonstrate a complete model for CO_2 hydrogenation to hydrocarbons via methanol route over an In_2O_3/HZSM-5 catalyst accompanied by a validation of the model through our experimental findings. An additional objective of the current work is to examine to what extent the combination of the two kinetic models can describe interactions between the reaction processes that result in, for example, suppression of the RWGS reaction and enhanced methanol/hydrocarbon yields compared to those obtainable with the methanol synthesis catalyst (In_2O_3) alone [6]. However, an examination of the deactivation kinetics of the zeolite is not included in the scope of this particular work.

2. Experimental

2.1. Catalyst preparation and characterization

The bifunctional catalytic bed used for this work consists of In_2O_3 and a commercially available HZSM-5 zeolite. The synthesis of In_2O_3 was carried out by a precipitation method that is reported in our previous work [21]. The HZSM-5, having a SiO_2/Al_2O_3 molar ratio of 23, was supplied in ammonium form by Zeolyst International (CBV 2314). The ammonium form zeolite was then calcined at 500 ℃ for 8 h to obtain the acidic form. Both the catalysts (In_2O_3 and HZSM-5) were individually pressed, crushed and sieved to granules ranging in size between 350 and 500 μm. Then the two catalysts, in their respective granule forms, were physically mixed in the mass ratio of In_2O_3:HZSM-5 = 2:1 and 3:1 respectively to make a total of 1.0 g of composite catalyst.

The morphology of the In_2O_3 and commercial HZSM-5 catalyst was examined using high resolution transmission electron microscopy (HRTEM) with an FEI Titan 80–300 instrument having an accelerating voltage of 300 kV. The crystalline structures of the pure and mixed samples were examined using X-ray diffraction (XRD) using a Bruker D8 X-ray diffractometer (see [21] for details). A Micromeritics Tristar 3000 instrument was used to determine the specific surface area and porous structure of the catalysts by nitrogen adsorption–desorption isotherms. Both the catalysts were degassed at 250 ℃ for 6 h under the nitrogen atmosphere.

2.2. Catalytic tests

Catalytic activity tests for the direct CO_2 hydrogenation reaction were performed using the different mass ratio mixtures of the catalysts in a high pressure continuous flow stainless steel reactor from VINCI Technologies, France. 1.0 g of the composite catalyst was loaded into the reactor (inner diameter = 12.7 mm and length = 215 mm) and fixed on either side with quartz wool and placed at the center position along the length of the vertically oriented reactor with a thermocouple tip penetrating slightly into the outlet end of the catalyst bed (bed height = 14 mm). This thermocouple monitored the temperature of the catalyst bed throughout the experiments, and it was found that the temperature difference between the setpoint furnace temperature and the actual reactor bed temperature was always less than 1℃. The remaining volume of the reactor, both upstream and downstream from the catalyst sample, was filled with 500 μm size inert carborundum (SiC) particles to evenly preheat the feed gas stream. The reactor was placed within a furnace. Before the reaction, the catalyst was pretreated in-situ at 400 ℃ for 1 h in pure Ar flow (150 Nml min^{-1}). After activation, the argon flow

was stopped and the reactant gas mixture of H_2/CO_2 in a 3:1 M ratio with a pressure of 40 bar gauge was introduced into the reactor. The estimated pressure drop over the catalyst bed was negligible (~0.001 bar from Ergun's equation) and hence it is reasonable to assume that the reactor was operated under isobaric conditions. Tests were conducted within a temperature range of 250 – 400 ℃, a total reactor gauge pressure varying between 20 and 40 bar, different H_2:CO_2 molar feed ratios varying from 1:1 to 4:1 and different weight hourly space velocities (WHSV) between 3000 and 7500 NmL $g_{cat}^{-1}h^{-1}$. The reactor gas effluents were quantitively analyzed using an online gas chromatograph (GC, SCION 456) with flame ionization (FID) and thermal conductivity detectors (TCD). The quantification and identification of each of the compounds (CO_2, CO, CH_4, CH_3OH and hydrocarbons) were performed based on calibration standards of known concentration. The concentrations measured by the GC were obtained after an average time of 2 h for a certain reaction condition to ensure that steady state conditions had been achieved. The composition of the hydrocarbons that are identified in the product stream using the FID detector of the GC consists of the following *lumps*: C_2-C_4 olefin (ethylene, propylene and butylene with its isomers), C_2-C_4 paraffin (ethane, propane, n-butane and *iso*-butane), C_5-C_8 (aliphatics and aromatics) and C_9^+ hydrocarbons (aliphatics and aromatics). Using the TCD, CO_2, CO, CH_4 and CH_3OH were detected. DME was never detected under any conditions in the effluent gas stream. The gas products from the reactor went through a condenser at room temperature and atmospheric pressure, where part of the water product condensed. Under all conditions used, the condensation of carbon containing products was considered negligible due to their high volatility and/or low concentration. All of the analysis results shown in this work were from the gas stream analyzed after the condenser. The possible condensation of water was also considered here and calculated.

The CO_2 conversion (X_{CO_2}), hydrocarbon distribution ($D_{C_nH_m}$) and selectivity (S_{HC}) and other product selectivities (e.g., CH_3OH, CO and CH_4) (S_i) were calculated according to the following equations:

$$X_{CO_2} = \frac{F_{CO_2,in} - F_{CO_2,out}}{F_{CO_2,in}} \times 100\% \tag{3}$$

where $F_{CO_2,in}$ and $F_{CO_2,out}$ are the molar flow rates of CO_2 at the inlet and outlet of the reactor respectively.

$$D_{C_nH_m} = \frac{nF_{C_nH_{m,out}}}{\sum_1^n nF_{C_nH_{m,out}}} \times 100\% \tag{4}$$

$$S_{HC} = \frac{\sum_1^n nF_{C_nH_{m,out}}}{F_{CO_2,in} - F_{CO_2,out}} \times 100\% \tag{5}$$

where $F_{C_nH_{m,out}}$ is the outlet molar flow rate of the hydrocarbon product C_nH_m formed and n is its corresponding carbon number.

$$S_i = \frac{F_{i,out}}{F_{CO_2,in} - F_{CO_2,out}} \times 100\% \tag{6}$$

where $F_{i,out}$ represents the outlet molar flow rates of product i (CH_3OH, CO, CH_4).

The carbon balance for an experiment was determined following the equation:

$$C_B = \frac{\sum_i nF_{i,out}}{F_{CO_2,in}} \times 100\% \tag{7}$$

where $F_{i,out}$ is the molar flow rate of species i at the outlet of the reactor.

Carbon balances were calculated for each experiment. Carbon balances were mostly greater than 92 % except at the highest reaction temperature of 400 ℃ where it dropped to 86 %. This might be because at higher temperatures more hydrocarbons were produced that became partially condensed but could not be specifically detected by experimental evidence since they are mixed with a large amount of water that also condenses at higher reaction temperatures.

2.3. Modeling methods

The reactor was modeled as a 1D pseudo-homogeneous plug flow reactor (as confirmed appropriately by a criterion based on the Bodenstein number as shown in the SI). In the simulations, it was assumed that the temperature and pressure were constant at steady-state conditions with negligible axial dispersion and the absence of mass transfer limitations for internal and external diffusion in the catalyst granules. All these conditions were estimated to have been satisfied for these direct CO_2 hydrogenation reactions. Isothermicity and negligible pressure drop in the bed have been already estimated and taken care of. Steady state measurements were ensured by the experimental procedure. Negligible mass transfer limitations in the catalyst granules were confirmed with the Mears and Weisz-Prater parameters calculated individually for both In_2O_3 and HZSM-5 catalysts for varying reaction temperatures as shown in the SI (Fig. S2). By doing a mass balance over a differential disc section of the catalyst bed, the mass balance equation is given by:

$$\frac{dF_j}{dw} = \sum_{i=1}^{n} \nu_{ij} \cdot r_{i,In_2O_3} \cdot \propto_{In_2O_3} + \sum_{i=1}^{n} \nu_{ij} \cdot r_{i,\mathrm{HZSM-5}} \cdot \propto_{HZSM-5} \tag{8}$$

where F_j is the molar flow rate of species j , w is the total catalyst weight, $\propto_{In_2O_3}$ is the mass fraction of In_2O_3 in the catalytic bed, $\propto_{HZSM-5}$ the mass fraction of HZSM-5 in the catalyst, ν_{ij} is the stoichiometric coefficient of species j in reaction i , r_{i,In_2O_3} is the rate of reaction i on In_2O_3 and $r_{i,\mathrm{HZSM-5}}$ is the corresponding reaction rate on the HZSM-5 zeolite. Since there are many species and reactions involved in the direct CO_2 hydrogenation to hydrocarbons over the In_2O_3/HZSM-5 bifunctional catalytic bed, eq. (8) yields a system of ordinary differential equations that are solved with the initial conditions (at $w = 0$) at the reactor inlet.

The optimization of the kinetic parameters in the model was done by minimizing the residual sum of squares (SSR) given by:

$$SSR = \sum_i \sum_j w_i \left(y_{i,j}^{exp} - y_{i,j}^{sim}\right)^2 \tag{9}$$

where w_i is the weighting factor for species i , $y_{i,j}^{exp}$ is the experimental mole fractions of the species i in experiment j and $y_{i,j}^{sim}$ is the corresponding estimated mole fraction from the solution of Eq. (8) using the ode15s solver in Matlab R2019b (MathWorks, Inc.). w_i is used as the weighting factor. SSR minimization was done using the 'lsqnonlin' subroutine function in the Matlab optimization package. All components but H_2 and H_2O were included in the optimization. The parameters tuned to minimize SSR are the kinetic parameters calculated using the following equations [21]:

$$k_i = k_{i,ref} \exp\left(\frac{E_i}{R}\left(\frac{1}{T_{ref}} - \frac{1}{T}\right)\right) \tag{10}$$

where $k_{i,ref}$ is the rate constant at the reference temperature T_{ref} , E_i is the activation energy and R is the gas constant. Eq. (10) is the Arrhenius equation in reparametrized form. The average temperature is 320 ℃ and is therefore used in the simulations.

Eq. (11) was used to determine the normalized sensitivity coefficients (S) for the parameters:

$$S = \beta_0 \frac{\sum \left(\frac{\Delta y^{sim}}{y_0^{sim}}\right)^2}{\Delta\beta} \tag{11}$$

where, β_0 is the optimal value of a parameter, $\Delta\beta$ is the change in parameter from its optimal value, y_0^{sim} is the simulated mole fraction value when the parameter is at its optimal value and Δy^{sim} is the change in simulated mole fraction when the parameter is changed from its optimal value. The normalized sensitivity coefficients evaluate the effect of each parameter on the simulation output. A parameter with a

relatively large sensitivity coefficient means that the parameter could be more accurately estimated from the data. But as the sensitivity coefficient is a relative measurement, there is no absolute value that should be achieved. In this work, all normalized sensitivity coefficients are calculated with a 0.1% change in each parameter value. An overview of all the experiments performed for the model validation is shown in Table S1.

3. Results and discussion

3.1. Catalyst characterization

The catalyst bed includes a metal oxide (In_2O_3) with a particle size of about 12 nm and a specific surface area of 103 $m^2\ g^{-1}$ and commercial HZSM-5 zeolite having a specific surface area of 376 $m^2\ g^{-1}$ mixed in different mass ratios and tested for the direct CO_2 hydrogenation reaction (Figs. S1b and c). The crystalline structure of pure In_2O_3 and HZSM-5 has been investigated and shown in Fig. S1a. HRTEM images of In_2O_3 (Fig. 1a and b) mostly showed spherical In_2O_3 particles with an exposed facet of (2 2 2). HZSM-5 having a lattice spacing of 1.0 nm corresponding to the (2 0 0) lattice plane is shown in the HRTEM images in SI (Figs. S1d and e).

3.2. Comparison of catalytic activities of pure In_2O_3 and In_2O_3/HZSM-5 bifunctional catalytic bed

The catalytic performance of the pure In_2O_3 catalyst has already been reported in our previous work [21]. It is interesting to compare the performance of the bifunctional catalytic bed to that of the same mass of pure In_2O_3 under the same reaction conditions as shown in Fig. 2. The catalysts were screened over a temperature range of 250–400 ℃ under the constant pressure of 40 bar, space velocity 6000 mL $g_{cat}^{-1}h^{-1}$ and feed molar H_2:CO_2 = 3:1. Fig. 2a and b show a comparison between the selectivity of methanol from the pure In_2O_3 catalyst and the methanol/hydrocarbon selectivity from the In_2O_3/HZSM-5 catalyst. From the two plots, it is evident that methanol was the major product having very high selectivity specifically at lower temperatures for the pure In_2O_3 catalyst. Whereas, for the bifunctional catalytic bed, it is clear that a major part of the methanol was converted over the zeolite to form hydrocarbons and hence the outlet methanol from the reactor is very low.

Comparing the CO_2 conversion in Fig. 2c, it was observed that for the bifunctional catalytic bed it is consistently slightly higher than that for pure In_2O_3 above 320 ℃. The differences at 320 ℃ and lower are minor and probably within the experimental accuracy. This higher CO_2 conversion at a higher temperature is also nicely consistent with the suggestion that the equilibrium limitation of the methanol synthesis is alleviated at higher temperatures, due to the near-complete consumption of methanol by the MTH reactions. Whereas, the use of the bifunctional catalytic bed reduced the CO selectivity significantly (as shown in Fig. 2c which is increasingly prominent at higher temperatures because of the suppression of the undesired RWGS reaction as has been pointed out earlier by Gao et al [1]. The CO selectivity data for pure In_2O_3 in Fig. 2c has been taken from our previous work with the pure In_2O_3 catalyst for CO_2 hydrogenation to methanol [21]. At 400 ℃, the CO selectivity reached 97 % for the pure In_2O_3 catalyst but it was reduced to around 49 % for the bifunctional catalytic bed under the same reaction conditions, with a minor increase in the CO_2 conversion. The lower CO selectivity results in a proportionately higher yield of methanol that was largely converted to hydrocarbons over the bifunctional catalytic bed compared to the higher methanol yield over the pure In_2O_3 catalyst. Over the bifunctional catalytic bed, in all cases, over 99 % of the methanol is converted to hydrocarbons resulting in less than 1% methanol selectivity at the reactor outlet at all temperatures (Fig. 2b). The methanol synthesis reaction over the pure In_2O_3 catalyst is exothermic and it was equilibrium limited from about 330 °C [21]. It is also known that both CH_3OH and CO formation competes for the consumption of the same reactants (CO_2 and H_2). So, at higher temperatures, the RWGS reaction, which is an endothermic reaction, dominates by lowering the reactant concentrations and produces large quantities of CO and water which hinders or even causes the reversal of the methanol synthesis over the pure In_2O_3 catalyst as reported by Ghosh et al. in our previous work [21]. However, over the In_2O_3/HZSM-5 bifunctional catalytic bed, the methanol yield is quite low at the reactor outlet due to its continuous consumption to form hydrocarbons over the HZSM-5 catalyst. Here the methanol synthesis reaction can occur with less equilibrium limitations and overcome the undesirable effects that the CO formation would have on its equilibrium. So, methanol formation that is unhindered consumes more reactants which can reduce the driving force and thus suppress the RWGS reaction to form CO [6] and also increase CO_2 conversion. Measurements at the standard reaction condition (320 ℃, 40 bar, 6000 mL$g_{cat}^{-1}h^{-1}$ and H_2:CO_2 = 3:1 M ratio) were repeated at periodic intervals during the whole experimental study at the same time as conversions and selectivities for other reaction conditions were measured. These repeated experiments exhibited only minor variations in CO_2 conversion and product selectivities during the whole study (Fig. S3). The absence of any systematic variations at the standard reaction conditions indicates that the catalyst was stable and can be considered to have been in a comparable state for the other reaction conditions tested throughout the study.

3.3. Proposed kinetic scheme and methodology for the kinetic study

To develop a kinetic model for CO_2 hydrogenation to hydrocarbon over the In_2O_3/HZSM-5 catalyst, the proposed kinetic scheme (Scheme

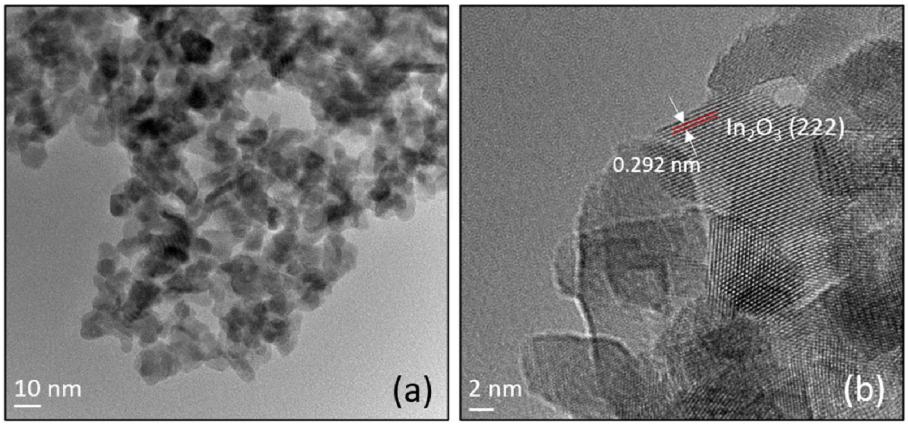

Fig. 1. HRTEM images of (a and b) synthesized In_2O_3 catalyst.

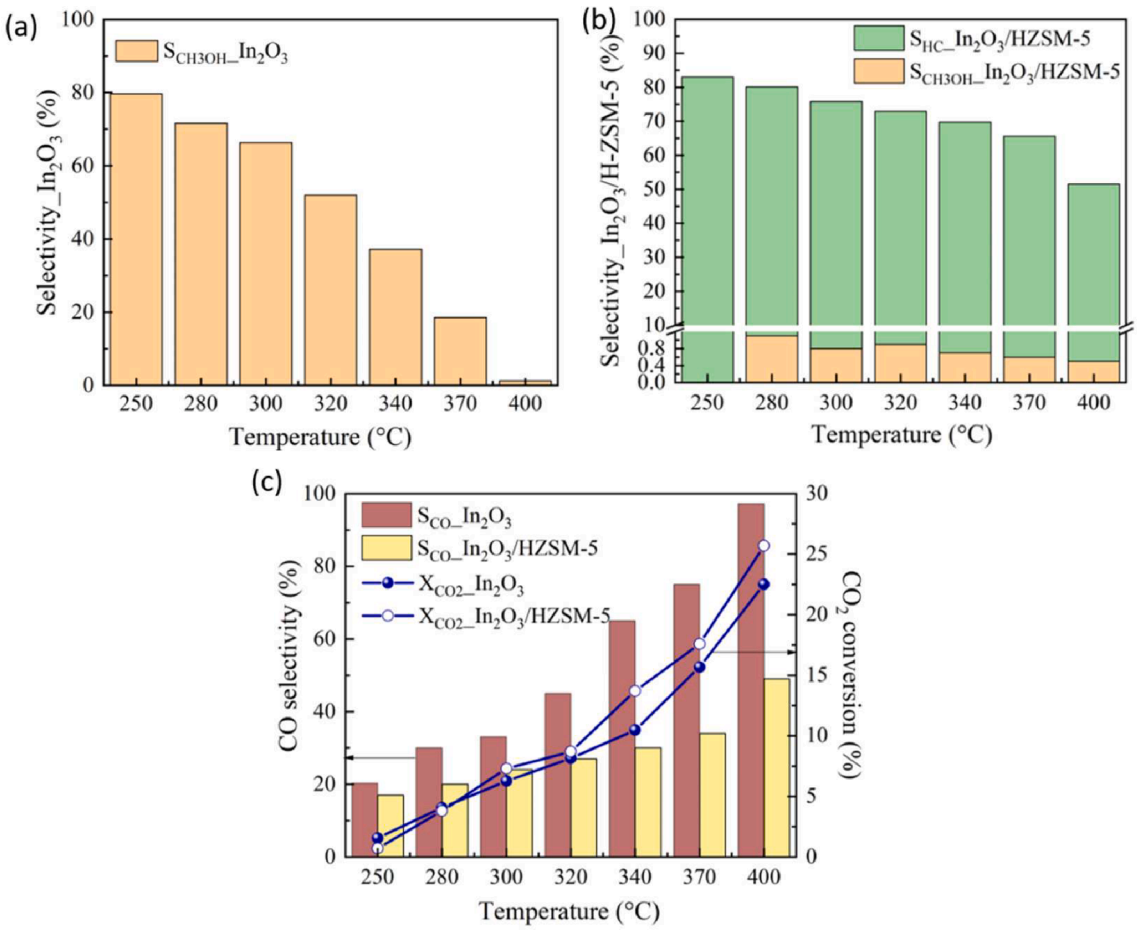

Fig. 2. Comparison of (a and b) selectivity of methanol from pure In_2O_3 [21] and methanol/hydrocarbon from In_2O_3/HZSM-5 and (c) CO_2 conversion and CO selectivity for 0.67 g pure In_2O_3 and bifunctional In_2O_3/HZSM-5, with 0.67 g In_2O_3 and 0.33 g HZSM-5. Compared under the same reaction conditions (40 bar, 6000 Nml h^{-1} feed flow rate of H_2:CO_2 = 3:1 M ratio).

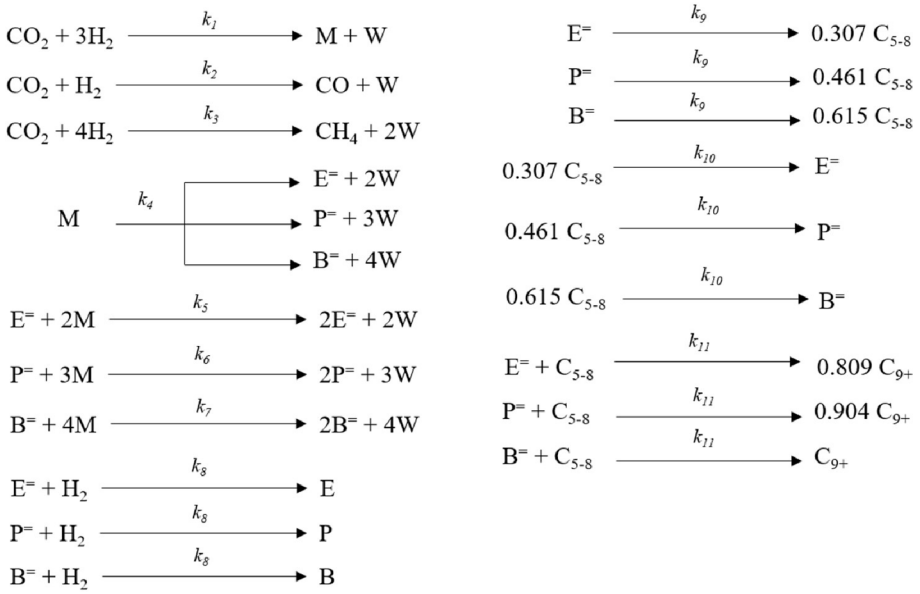

Scheme 1. Proposed kinetic scheme for the CO_2 hydrogenation to hydrocarbons over In_2O_3/HZSM-5 catalyst. M−methanol, W-water, E-ethane, P-propane, B-butane, $E^=$-ethene, $P^=$-propene, $B^=$-butene, C_{5-8}-lumped products with carbon numbers 5 to 8 and C_9^+-lumped products with carbon number greater than 9 (specifically between C_9 and up to C_{12}).

1) is based on a combination of the model developed by Ghosh et al. [21] for CO_2 hydrogenation to methanol over the In_2O_3 catalyst and a modified version of the *lump* type model developed by Pérez-Uriarte et al. [30] for the conversion of DME and methanol to olefins over an HZSM-5 zeolite. In the scheme, M stands for methanol, W for water, E, P and B for ethane, propane and butane respectively and $E^{=}$, $P^{=}$ and $B^{=}$ for ethylene, propylene and butylene respectively, $C_{5\text{-}8}$ are the products with carbon numbers 5 to 8 lumped together and C_9^+ are the lumped products with carbon number greater than 9 (specifically between C_9 and up to C_{12}) detected using GC. The reaction steps for CO_2 to CH_3OH and CH_3OH to hydrocarbons as presented in Table 1 have been considered.

Among these reactions, reactions 1–3 occur over the In_2O_3 catalyst and the remaining reactions 4–11 were considered to occur over the HZSM-5 zeolite. Some of the significant modifications made to the MTH model by Pérez-Uriarte et al., when here combined with the methanol synthesis model, include:

(a) DME was not included as an intermediate from methanol to hydrocarbons.
(b) Hydrogenation reaction (8) was included for the formation of C_2-C_4 paraffins.
(c) Aromatics are not considered separately as products and are instead included in the C_5-C_8 and C_{9+} lumps.
(d) Cracking reactions converting the $C_{5\text{-}8}$ lump back to $C_{2\text{-}4}$ olefins were included as reaction (10).
(e) The model was extended to include the formation of a C_{9+} lump of products as reaction (11).

Table 1
Summary of the reactions used in the kinetic modeling:

Reaction number	Reaction	Description
1	$CO_2 + 3H_2 \rightleftharpoons CH_3OH + H_2O$	Methanol synthesis
2	$CO_2 + H_2 \rightleftharpoons CO + H_2O$	RWGS reaction
3	$CO_2 + 4H_2 \rightleftharpoons CH_4 + 2H_2O$	Methanation
4	$2CH_3OH \rightarrow C_2H_4 + 2H_2O$	Ethylene formation from methanol
4	$3CH_3OH \rightarrow C_3H_6 + 3H_2O$	Propylene formation from methanol
4	$4CH_3OH \rightarrow C_4H_8 + 4H_2O$	Butylene formation from methanol
5	$C_2H_4 + 2CH_3OH \rightarrow 2C_2H_4 + 2H_2O$	Autocatalytic growth of ethylene from methanol
6	$C_3H_6 + 3CH_3OH \rightarrow 2C_3H_6 + 3H_2O$	Autocatalytic growth of propylene from methanol
7	$C_4H_8 + 4CH_3OH \rightarrow 2C_4H_8 + 4H_2O$	Autocatalytic growth of butylene from methanol
8_1	$C_2H_4 + H_2 \rightarrow C_2H_6$	Ethylene hydrogenation to form ethane
8_2	$C_3H_6 + H_2 \rightarrow C_3H_8$	Propylene hydrogenation to form propane
8_3	$C_4H_8 + H_2 \rightarrow C_4H_{10}$	Butylene hydrogenation to form butane
9_1	$C_2H_4 \rightarrow 0.307C_{5-8}$	C_5 - C_8 formation from ethylene (oligomerization reaction)
9_2	$C_3H_6 \rightarrow 0.461C_{5-8}$	C_5 - C_8 formation from propylene (oligomerization reaction)
9_3	$C_4H_8 \rightarrow 0.615C_{5-8}$	C_5 - C_8 formation from butylene (oligomerization reaction)
10_1	$0.307C_{5-8} \rightarrow C_2H_4$	C_5 - C_8 cracking to ethylene
10_2	$0.461C_{5-8} \rightarrow C_3H_6$	C_5 - C_8 cracking to propylene
10_3	$0.615C_{5-8} \rightarrow C_3H_6$	C_5 - C_8 cracking to butylene
11_1	$C_2H_4 + C_{5-8} \rightarrow 0.809C_{9+}$	C_{9+} formation from ethylene and C_5 - C_8
11_2	$C_3H_6 + C_{5-8} \rightarrow 0.904C_{9+}$	C_{9+} formation from propylene and C_5 - C_8
11_3	$C_4H_8 + C_{5-8} \rightarrow C_{9+}$	C_{9+} formation from butylene and C_5 - C_8

Reaction steps for methanol dehydrating to form DME and simultaneously DME forming hydrocarbons have not been included in this model since DME could never be detected experimentally at the reactor outlet at the experimental conditions used. This precluded any possibility to accurately determine the kinetic parameters for the formation and consumption of DME. This does not mean that these reactions do not occur over this catalyst. DME is known to react faster than CH_3OH to form olefins over HZSM-5 zeolite as reported by Pérez-Uriarte et al. in literature [30], so this simply means that DME was undetectable at our reaction conditions with CH_3OH only present in very lower concentrations (see Fig. 2b). So, for our reaction conditions, we consider that the DME formed is consumed quickly to form the hydrocarbons. However, in the SI (Tables S2 and S3 and Fig. S4), we have shown that adding the reactions containing DME with kinetic parameters as reported by Pérez-Uriarte et al. [30] to our final model had little effect on the fitting of the model to the experimental data.

Hydrogen is present as a reactant in this system and therefore the yield of paraffin products was much higher at these conditions compared to studies where methanol/DME converts to hydrocarbons in the absence of hydrogen [31]. Also, it is known that olefin hydrogenation reactions are catalyzed by acidic zeolites [32], however, any reports of olefin hydrogenation over In_2O_3 catalysts are lacking in the literature. In order not to further complicate the model and introduce large correlations between reactions, we have added reactions for hydrogenation of olefins only on the zeolite (reaction (8)). In addition, our results with varying the mass ratio of the catalyst components show that the model predictions of the ratio of saturated and unsaturated hydrocarbons did not differ significantly from the experiments, which suggests that at the experimental conditions examined, the olefin hydrogenation over the oxide catalyst was negligible. In a later section, it will be shown that there was some diminishing yield of higher hydrocarbons at elevated temperatures and it is well known that cracking reactions occur over the acid zeolites [6]. Hence, it was necessary to add the cracking reactions to form the lower olefins back from the higher hydrocarbons. The stoichiometric coefficients of reactions (9) and (10) are calculated based on the average carbon number for that particular product lump. E.g. for reaction 9_1 the stoichiometric coefficient was calculated as 2 (carbon number for ethylene)/6.5 (average carbon number of the lump C_5-C_8) = 0.307. The stoichiometric coefficients for reactions 9_2, 9_3 and $10_{1\text{-}3}$ have been calculated in a similar way. On the other hand, for reaction 11_1 the coefficients are calculated as (2 (carbon number for ethylene) + 6.5 (average carbon number for $C_{5\text{-}8}$ lump))/10.5 (average carbon number of the lump C_9-C_{12}) = 0.809. The other two coefficients for reaction (11) are also calculated in the equivalent way.

As in the original model of Pérez-Uriarte et al. [30], all reactions producing the same product lumps are considered to have the same rate constants. For example, olefin formation from methanol reactions have been lumped together since they should have identical rate determining steps and have the same rate constant k_4 . Similar *lumps* (with identical rate constants) for the hydrogenation of olefins to form paraffin (k_8), C_5-C_8 formation from olefins (k_9), C_5-C_8 cracking (k_{10}) and C_9^+ formation (k_{11}) have been considered (see Scheme 1). The consumption of the different olefins was however not exactly the same and the different reactivities of each olefin are considered by using f_i consumption factors expressing the reactivities of ethylene and butylene relative to that of propylene.

The rate equations (Eqs. 12–22) considered for the combined model based on the equations shown in Table 1 are as follows:

$$r_1 = \frac{k_1 \frac{\left(P_{CO_2}.{P_{H_2}}^3 - \frac{P_{CH_3OH}.P_{H_2O}}{K_{eq,1}}\right)}{{P_{H_2}}^2}}{I_{In2O3}} \quad (12)$$

$$r_2 = \frac{\frac{k_2}{\sqrt{P_{H_2}}}\left(P_{CO_2}.P_{H_2} - \frac{P_{CO}.P_{H_2O}}{K_{eq,2}}\right)}{I_{In2O3}} \quad (13)$$

$$r_3 = k_3\sqrt{P_{CO_2}}\sqrt{P_{H_2}}\,\frac{\left(1 - \frac{P_{CH_4}.P_{H_2O}^2}{P_{CO_2}P_{H_2}^4 K_{eq,3}}\right)}{I_{In2O3}} \quad (14)$$

$$r_4 = k_4\frac{P_{CH_3OH}}{I_{HZSM-5}} \quad (15)$$

$$r_5 = k_5\frac{P_{CH_3OH}\bullet P_{C_2H_4}}{I_{HZSM-5}} \quad (16)$$

$$r_6 = k_5\frac{P_{CH_3OH}\bullet P_{C_3H_6}}{I_{HZSM-5}} \quad (17)$$

$$r_7 = k_5\frac{P_{CH_3OH}\bullet P_{C_4H_8}}{I_{HZSM-5}} \quad (18)$$

$$r_8 = k_8\frac{P_{C_2H_4/C_3H_6/C_4H_8}\bullet P_{H_2}}{I_{HZSM-5}}\bullet f_{i\_8} \quad (19)$$

$$r_9 = k_9\frac{P_{C_2H_4/C_3H_6/C_4H_8}}{I_{HZSM-5}}\bullet f_{i\_9} \quad (20)$$

$$r_{10} = k_{10}\frac{P_{C_5\_C_8}}{I_{HZSM-5}}\bullet f_{i\_9} \quad (21)$$

$$r_{11} = k_{11}\frac{P_{C_2H_4/C_3H_6/C_4H_8}\bullet P_{C_5\_C_8}}{I_{HZSM-5}}\bullet f_{i\_9} \quad (22)$$

where P_i is the partial pressure of the species i , f_i is the olefin consumption factor ($i = 1, 2$ for ethylene and butylene respectively), k_j (in mol s^{-1} kg_{cat}^{-1}) is the rate constant of reaction j and $K_{eq,j}$ (in bar^{-1}) is the thermodynamic equilibrium constant for reaction j . In r_8 , r_9 and r_{11} , the partial pressures vary depending on the species being hydrogenated but the reaction rate constants are the same regardless of the species since they are lumped together. The kinetic rate equations r_1 through r_3 have been directly taken from our previous CO_2 to CH_3OH model where they were developed based on an LHHW kinetic mechanism for the same In_2O_3 catalyst [21]. CO_2 and H_2 are considered to adsorb initially on the In_2O_3 surface where H_2 adsorbs dissociatively to form methanol and water which thereafter desorb from the HZSM-5 zeolite surface. The inhibition terms over In_2O_3 (I_{In2O3}) and HZSM-5 (I_{HZSM-5}) are as follows:

$$I_{In2O3} = \left(1 + K_{CO_2}.P_{CO_2} + \sqrt{K_{H_2}.P_{H_2}}\right)^2 \quad (23)$$

$$I_{HZSM-5} = 1 + K_{CH_3OH}(P_{CH_3OH} + P_{H_2O}) \quad (24)$$

where K_{CO_2} , K_{H_2} , K_{CH_3OH} are the adsorption equilibrium constants for CO_2, H_2 and CH_3OH respectively.

3.4. Kinetic parameters and comparison with other models

The kinetic parameters derived by Ghosh et al. for CO_2 hydrogenation to methanol over In_2O_3 catalyst have been directly used in this work [21]. The In_2O_3 catalyst material used for this particular work is the same as used in our previous work. It is unlikely that the In_2O_3 catalyst in granule form has changed in composition when physically mixed with the HZSM-5 (also in granule form) to make the bifunctional catalytic bed. It is, therefore, reasonable to consider that the kinetic parameters from Ghosh et al. [21] should apply here. For our model, wherever possible, the original parameter values were directly used from the model by Pérez-Uriarte et al. [30] as starting estimates. For a comparison of those two models with other CO_2 to methanol and MTO kinetic models, we refer to the original publications [21,30]. However, if the model predictions were sensitive to the parameter value, they were tuned to fit the experimental data. For the reactions added to the original kinetic model, their parameter values of course needed to be estimated by directly tuning to the experimental data. Kinetic parameter values reported by Pérez-Uriarte et al. could not, in most cases, be used directly because of the following reasons:

a) The zeolite HZSM-5 used in this particular work has a different SiO_2/Al_2O_3 ratio (23) than the one used in their work (280) and hence the acid site density in the two zeolites vary significantly.
b) Also, most importantly, the reaction conditions used in this work are quite different from those in the work of Pérez-Uriarte et al. In this particular work, methanol and DME are present in much lower concentrations since they are reaction intermediates, instead of the main reactants.
c) CO_2 and H_2 both are present as feed in our reactions. The presence of hydrogen with high partial pressure should cause the hydrogenation of lower olefins and this hinders the formation of higher molecular weight products since then the oligomerization reactions are not possible.

On the other hand, the parameter values for the inhibition term for methanol and water on the zeolite were taken directly from Pérez-Uriarte et al. [30] since the experimental data in the present study was insufficient to resolve the adsorption/desorption equilibrium of methanol and water. Also, there was no reason anyway to suspect that equilibrium adsorption would be different on the acid sites of the HZSM-5 used in this study.

Any kinetic parameter with a high normalized sensitivity coefficient indicates that the experiments were well suited to accurately resolve that particular parameter. The reaction rate constants in Table 2 for CH_3OH, CO and CH_4 reported by Ghosh et al. in their CO_2 to methanol model have been directly utilized for reactions 1–3 in Table 1 for the CO_2 hydrogenation to hydrocarbon model, keeping in mind that the reference temperature used in the previous work was 300 °C, whereas here it is 320 °C [21]. The remaining reactions (reactions 4–11) for the MTH part have been adopted from the DME/methanol to olefin model by Pérez-Uriarte et al. [30], of course with necessary modifications as described earlier. The values of the rate constants and activation energies (in Table 2) of the two lumped reactions: olefin formation reactions from methanol (reaction (4)) and C_5-C_8 formation from olefins (reaction (9)) have been adjusted from those reported by Pérez-Uriarte et al. [30] to improve the fit with our experimental data. The values of two additional reactions (reactions (10) and (11)) are also tuned according to our experimental results. The autocatalytic reactions (reactions 5–7) adopted from the model by Pérez-Uriarte et al. were of little

Table 2
Rate constants and activation energies optimized using lsqnonlin, for the direct CO_2 hydrogenation to hydrocarbon kinetic model over In_2O_3/HZSM-5 catalyst including their sensitivity coefficients.

Reaction number	* k_{ref} (mol s^{-1} bar^{-1} kg_{cat}^{-1}) at 320 °C	Normalized sensitivity	E_a (kJ mol^{-1})	Normalized sensitivity
1	8.8×10^{-4a}	2.7×10^{-1}	35.7^a	1.1×10^{-2}
2	2.6×10^{-3a}	1.8×10^{-2}	54.5^a	1.4×10^{-9}
3	1.4×10^{-4a}	1.8×10^{-2}	42.5^a	7.3×10^{-9}
4	5.9×10^{-1c}	1.7×10^{-2}	70.0^c	1.5×10^{-9}
5	7.0×10^{-2b}	3.4×10^{-8}	16.0^b	8.6×10^{-2}
6	6.0×10^{-1b}	1.3×10^{-7}	17.0^b	6.2×10^{-2}
7	5.9×10^{-2b}	7.5×10^{-9}	69.0^b	3.1×10^{-2}
8	8.0×10^{-2c}	5.6×10^{-2}	109.0^c	1.1×10^{-3}
9	8.3×10^{-1c}	2.6×10^{-2}	150.0^c	4.6×10^{-2}
10	6.0×10^{-2c}	4.0×10^{-2}	170.0^c	4.1×10^{-1}
11	8.2×10^{-1c}	1.7×10^{-2}	25.0^c	4.2×10^{-2}

a: value taken from [21], *b*: value taken from [30], *c*: value tuned to the current experimental data.

significance for our model, as indicated by their low sensitivity coefficients, and hence their rate constants were not well resolved under our experimental conditions. Methanol was present in only very low concentrations under our reaction conditions and hence it is probable that the autocatalytic reactions are of lesser importance in this case. Excluding the autocatalytic and the methanol to olefin reactions, the normalized sensitivity coefficients for all other rate constants could be well resolved from this model under our experimental conditions. The activation energy for methanol to olefin (reaction (4)) could not be accurately resolved from this model as can be seen from its low normalized sensitivity coefficient. Again, the low concentration of methanol can be a probable reason behind such a low sensitivity.

Moreover, the adsorption equilibrium constants and the enthalpies of adsorption for CO_2 and H_2 presented in Table 3, for methanol synthesis on In_2O_3, are also the same as those reported by Ghosh et al [21]. The adsorption equilibrium constants and enthalpy of adsorption for CH_3OH/H_2O have been taken directly from the DME/methanol to olefin model developed by Pérez-Uriarte et al. [30], keeping in mind that they were reported at 350 ℃, whereas our reference temperature here is 320 ℃. Since no feeding of methanol or water was done in this work, to examine the inhibiting effects of water and methanol on MTH, the normalized sensitivity coefficients for $\Delta H_{CH_3OH/H_2O}$ is especially low.

The DME/methanol to olefin model by Pérez-Uriarte et al. [30] also includes DME as the main feed. For our experiments, we could not detect any DME in our reactor outlet as mentioned earlier since it is one of our reaction intermediates. So, the reactions involving DME were excluded in our adapted model. Table S4 shows the consumption factors (f_i) for ethylene and butylene w.r.t propylene used in this model for the rate equations $r_8 - r_{11}$ along with their normalized sensitivity coefficients. The values indicate that these parameters could be resolved well from our experiments.

3.5. Comparison between experimental results and kinetic model predictions

To validate the proposed kinetic model, the experimental results (points) and those calculated by the model (lines) showing the mole fractions of different products formed during the CO_2 hydrogenation reaction at different temperatures, pressures, molar feed ratios and space velocities over the In_2O_3/HZSM-5 (2:1 mass ratio) catalyst are plotted and compared in Figs. 3 to 6 respectively. A wide range of reaction parameters have been considered and the goodness of the fit is observed. Deviations have been observed for all experiments at the highest temperature (400℃). The main reason behind these deviations can be the poorer carbon balance that was observed in the experimental results at the highest temperature, but possible changes in the reaction kinetics unexplained by the model at the highest temperature cannot be excluded.

The effect of reaction temperature on the product distribution for CO_2 hydrogenation to hydrocarbon was studied over the temperature range from 250 to 400 ℃. Methanol is dehydrated to form olefins and these olefins through oligomerization reactions form higher hydrocarbons. Due to the high hydrogen partial pressure, a significant portion of the olefins is hydrogenated to form paraffin. Fig. 3 shows the variation of the mole fractions of different products (CH_3OH, CO, CH_4, C_2-C_4 paraffin, C_2-C_4 olefin, C_5-C_8 and C_9^+ hydrocarbons) at the reactor outlet w.r.t. reaction temperature. The model predicts that methanol concentration first increases with temperature and then after 350℃, it starts to reduce. But experimentally we observed an increase in methanol concentration up to 400℃ over the In_2O_3: HZSM-5 catalyst. On the other hand, CO and CH_4 continuously increase with temperature as was also observed in the CO_2 to methanol model by Ghosh et al [21]. The mole fractions of CH_3OH, CO and CH_4 are slightly over-predicted by the model as can be seen from Fig. 3b and 3c. The main reason behind this is that, in the combined model we have retained the exact values of all the kinetic parameters for the formation of CH_3OH, CO and CH_4 as reported by Ghosh et al. in their previous work for the CO_2 to methanol model. This methanol synthesis model does not account for the possible inhibiting effects of higher water concentration and the presence of hydrocarbons over the pure In_2O_3 catalyst. The inhibiting effect of water for methanol synthesis over In_2O_3 is known due to its observed negative reaction order [33] and one can suspect that hydrocarbons, and in particular olefins, could also have inhibiting effects although not yet studied.

But some significant points need to be mentioned here. Firstly, it has been observed that the combined model predicts a much lower concentration of methanol, compared to that without the HZSM-5 catalyst, at the outlet which is quite obvious since most of the methanol is utilized to form hydrocarbons over the zeolite. Moreover, the model can also predict a significant reduction in CO concentration in the product that fits well with the experimental findings as already discussed in Fig. 2c. With the increase in temperature, the mole fractions of paraffin increase but for olefins, they initially increase but reduce at higher temperatures. With the increase in temperature, the total mole fraction of C_2-C_4 increases and C_5-C_8 first increases and at higher temperature reduces. Very small traces of C_9^+ higher hydrocarbons were obtained.

All the hydrocarbon yields increase with the increase in total reactor pressure (see Fig. 4). The main reason behind this is that an increase in total pressure favors methanol formation thermodynamically, but the equilibrium for the RWGS reaction remains unaltered by pressure [21]. So, more methanol is available for the acidic sites of the zeolite HZSM-5 that can be converted to hydrocarbons as the pressure increases from 20 to 40 bar. Similar features were also observed as we increased the molar H_2:CO_2 ratio from 1:1 to 4:1 (Fig. 5). Gao et al. reported that higher pressure and H_2/CO_2 ratio can enhance the CO_2 conversion and reduce CO selectivity thereby increasing the net yield of hydrocarbons over the bifunctional catalytic bed [1]. The experimental data under these conditions corresponded well with our model predictions.

Both methanol and CO mole fractions reduced as the space velocity was increased (Fig. 6b and 6c) and this is consistent with the CO_2 to methanol model reported by Ghosh et al [21]. The space velocity was varied from 3000 − 7500 mL $g_{cat}^{-1}h^{-1}$ by varying the flow rates of the reactant gases and keeping the weight of the catalyst constant. Less methanol is available for the acidic sites of HZSM-5 resulting in the reduction of the mole fraction of hydrocarbons from the In_2O_3/HZSM-5 catalyst (Fig. 6d, 6e and 6f). Our model corresponds well with the experimental data obtained by the variation of space velocities as can be seen from Fig. 6.

Further, we have compared the CO_2 conversion and product selectivities along with the hydrocarbon distribution as calculated from the experimental data and the simulated results from the model in Fig. 7. When we compare Fig. 7a and 7c, we can see that both the experimental and simulated results showed similar trends for CO_2 conversion and product selectivities over In_2O_3/HZSM-5 (2:1) catalyst. Both CO_2 conversion and CO selectivity increase with temperature and the hydrocarbon selectivity gradually reduce with temperature.

The experimental data shows slightly higher hydrocarbon selectivity and lower CO selectivity in comparison to that predicted by the model.

Table 3
Adsorption equilibrium constants (at 320 ℃) and heat of adsorption for the final model and their normalized sensitivity coefficient.

Parameter	Value	Unit	Normalized sensitivity
$K_{CO_2,ref}$	6.7×10^{-1a}	bar^{-1}	4.6×10^{-3}
$K_{H_2,ref}$	7.0×10^{-1a}	bar^{-1}	2.2×10^{-2}
$K_{CH_3OH/H_2O,ref}$	1.3×10^{1b}	bar^{-1}	3.4×10^{-3}
ΔH_{CO_2}	-2.6×10^{1a}	kJ mol^{-1}	2.1×10^{-2}
ΔH_{H_2}	-1.2×10^{1a}	kJ mol^{-1}	3.6×10^{-3}
$\Delta H_{CH_3OH/H_2O}$	-2.0×10^{-1b}	kJ mol^{-1}	1.3×10^{-7}

a: value taken from [21], *b*: value taken from [30].

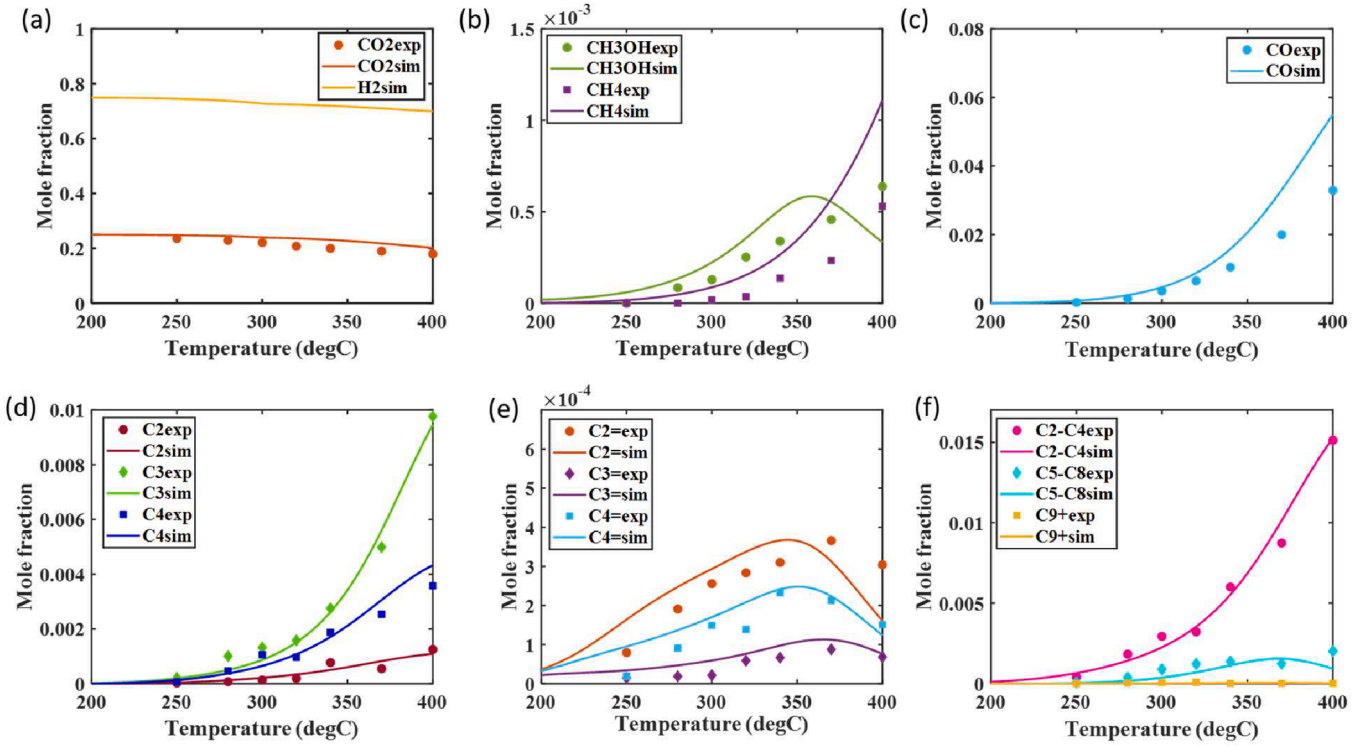

Fig. 3. The outlet mole fractions as a function of temperature for (a) CO_2 and H_2, (b) CH_3OH and CH_4, (c) CO, (d) C_2-C_4 paraffin, (e) C_2-C_4 olefin and (f) lumped hydrocarbons for In_2O_3/HZSM-5 = 2:1. The symbols represent the experiments and the lines represent simulations. The experiments are performed at the following conditions: 40 bar, 6000 mL $g_{cat}^{-1}h^{-1}$ and H_2:CO_2 = 3:1 M ratio.

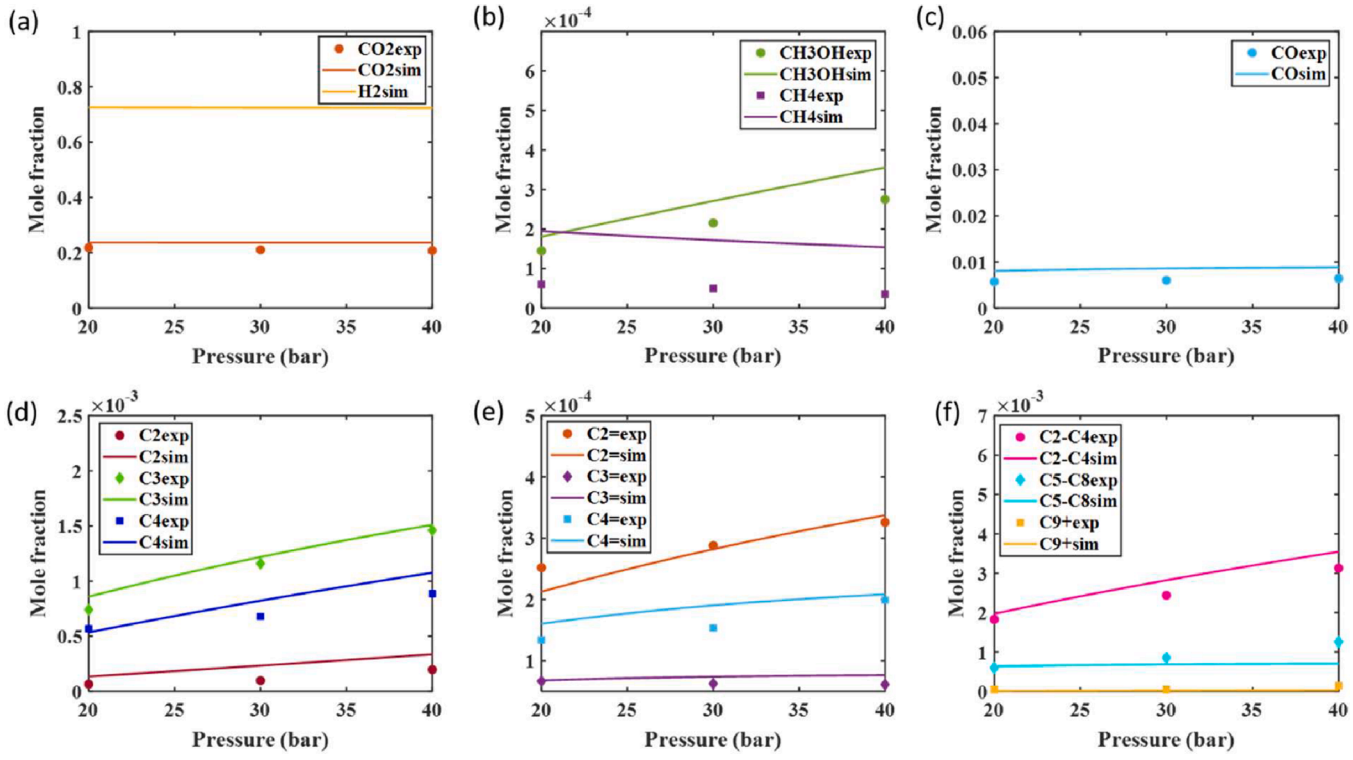

Fig. 4. The outlet mole fractions as a function of pressure for (a) CO_2 and H_2, (b) CH_3OH and CH_4, (c) CO, (d) C_2-C_4 paraffin, (e) C_2-C_4 olefin and (f) lumped hydrocarbons for In_2O_3/HZSM-5 = 2:1. The symbols represent the experiments and the lines represent simulations. The experiments are performed at the following conditions: 320 ℃, 6000 mL $g_{cat}^{-1}h^{-1}$ and H_2:CO_2 = 3:1 M ratio.

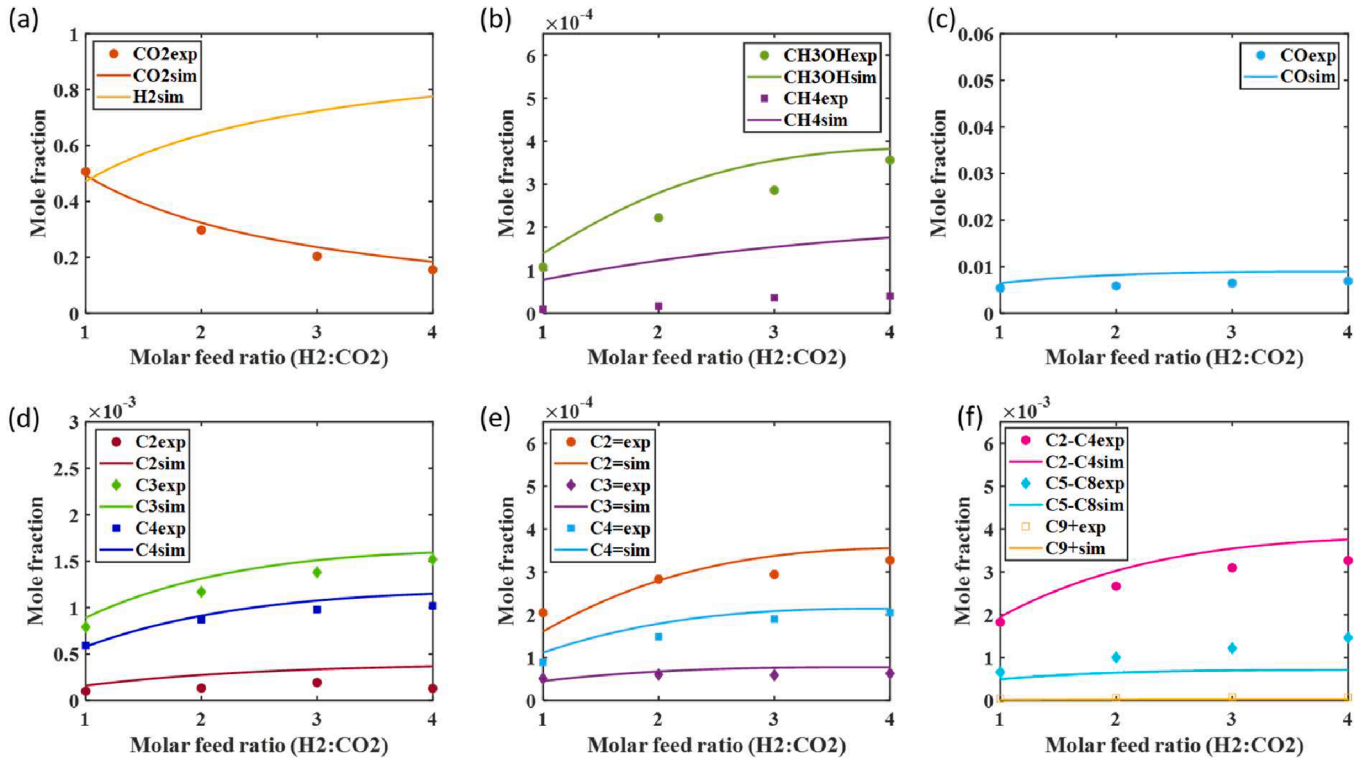

Fig. 5. The outlet mole fractions as a function of molar feed ratio for (a) CO_2 and H_2, (b) CH_3OH and CH_4, (c) CO, (d) C_2-C_4 paraffin, (e) C_2-C_4 olefin and (f) lumped hydrocarbons for In_2O_3/HZSM-5 = 2:1. The symbols represent the experiments and the lines represent simulations. The experiments are performed at the following conditions: 320 ℃, 40 bar and 6000 mL $g_{cat}^{-1}h^{-1}$.

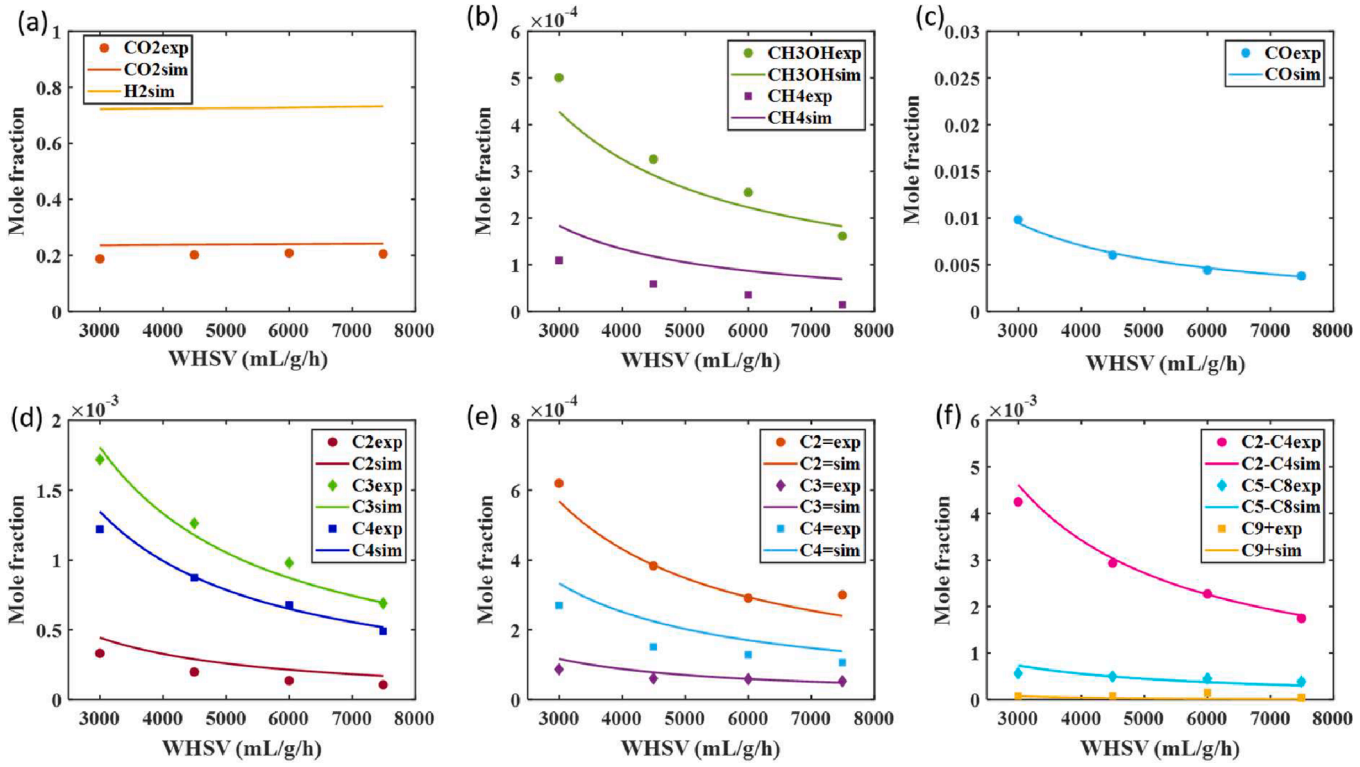

Fig. 6. The outlet mole fractions as a function of space velocity for (a) CO_2 and H_2, (b) CH_3OH and CH_4, (c) CO, (d) C_2-C_4 paraffin, (e) C_2-C_4 olefin and (f) lumped hydrocarbons for In_2O_3/HZSM-5 = 2:1. The symbols represent the experiments and the lines represent simulations. The experiments are performed at the following conditions: 320 ℃, 40 bar and H_2:CO_2 = 3:1 M ratio.

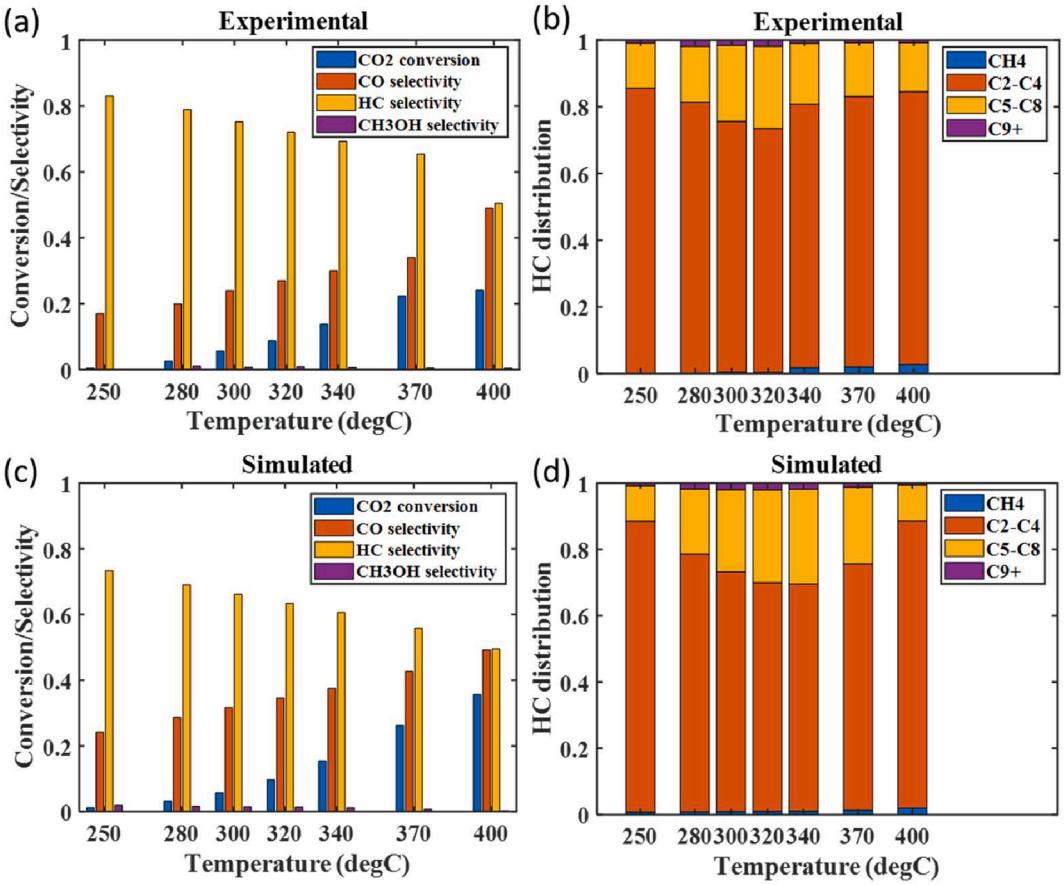

Fig. 7. Comparison between (a and b) experimental and (c and d) simulated CO_2 conversion, product selectivities and hydrocarbon distribution for In_2O_3/HZSM-5 = 2:1 catalyst. Reaction conditions: 40 bar, 6000 mL $g_{cat}^{-1}h^{-1}$ and H_2:CO_2 = 3:1 M ratio in the feed.

The slightly higher CO selectivity predicted by the model corresponds to the higher CO mole fraction shown in Fig. 3c. On the other hand, the maximum CO_2 conversion predicted by the model at 400 ℃ is 35 %, but experimental results show that 25 % CO_2 conversion could be obtained at the same temperature. A 49 % CO selectivity was predicted both by the model as well as by the experimental results at 400 ℃. All these data nicely depict that the model can well predict the experimental data for direct CO_2 hydrogenation to hydrocarbons over In_2O_3/HZSM-5 (2:1) catalyst. In addition, when the hydrocarbon distribution between the experimental data and that predicted by the model is compared (Fig. 7b and 7d), it is seen that the trend of hydrocarbon distribution predicted by the model matches well with that from the experiments. C_5^+ hydrocarbon selectivity gradually increases and then decreases with the increase of reaction temperature over the bifunctional catalytic bed.

At higher temperatures, the cracking of higher hydrocarbons, specifically, the C_5-C_8 product lump, increases (reaction (10) in Table 1) to form lower olefins and hence the selectivity of C_2-C_4 increases with temperature. This is assisted by the fact that the activation energy of reaction (10) is greater than that for reaction (9), as evident in Table 2. A maximum C_5^+ hydrocarbon yield was obtained at around 320 ℃ both from the model prediction as well as experimentally. Around 27 % of C_5^+ hydrocarbon was obtained from the experimental results whereas the model predicted around 30 %. 1.8 % C_9^+ was obtained experimentally whereas the model predicts 2 % C_9^+ hydrocarbons at 320 ℃ for the In_2O_3/HZSM-5 = 2:1 catalyst.

3.6. Model validation and comparison in performance between two different catalyst mass ratios

After developing the kinetic model for direct CO_2 hydrogenation to hydrocarbons over the In_2O_3/ HZSM-5 bifunctional catalytic bed using the experimental data from the In_2O_3/HZSM-5 mass ratio of 2:1, the variation of the model predictions with a change in the mass ratio of the catalyst was used to validate the model (by using exactly the same kinetic parameters as utilized by the In_2O_3/ HZSM-5 = 2:1 mass ratio). So, the influence of an increase in the catalyst mass ratio to In_2O_3/HZSM-5 = 3:1 (maintaining the total catalyst weight = 1 g) from mass ratio 2:1 was examined. In this aspect, Fig. S5 in the SI shows the mole fractions of different products formed from the In_2O_3/HZSM-5 (3:1) with the variation of reaction temperature. There is more In_2O_3 for the In_2O_3/HZSM-5 = 3:1 ratio catalyst when compared to the 2:1 mass ratio. Hence, this catalyst produces 60 % more methanol (at 320 ℃) than that formed with the mass ratio of 2:1 according to the experiments. The effect of pressure, molar feed ratio and space velocity on the 3:1 mass ratio catalyst as predicted by the model as well as validated by experimental results are shown in Fig. S5-S8 in the SI. The CO_2 conversion and product selectivities between the experimental and the simulated results for the In_2O_3: HZSM-5 (3:1) catalyst matched well supporting the validity of the model as shown in Fig. S9 (a and c). HC selectivities slightly reduce and CO selectivity increases for the 3:1 mass ratio catalyst when compared to the 2:1 mass ratio. The experimental hydrocarbon distribution also was sensitive towards the mass ratio of the catalysts as can be seen from Fig. S9 (b and d). But the trend seemed to be the same as the experimental findings where it is seen that the selectivity for C_5^+ hydrocarbons gradually increased with temperature up to around 340 ℃ after which it started to decrease as temperature increased.

A comparison between the model predictions and experimental findings for the two different mass ratios of catalysts is shown in detail in Fig. 8. From Fig. 8 (a and d), it can be seen that both the model prediction and the experimental findings confirm the fact that methanol

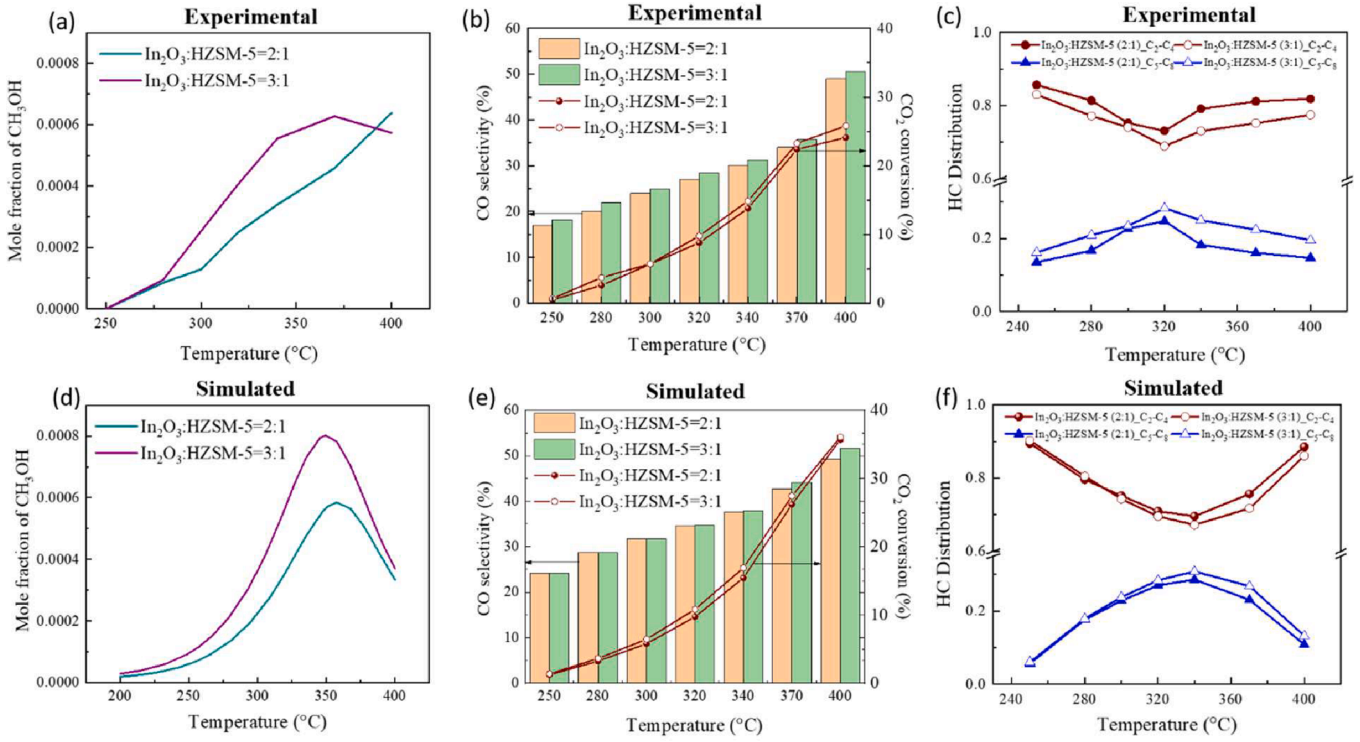

Fig. 8. Comparison between model predictions and experimental results with different catalyst mass ratios for (a and d) mole fraction of methanol formed, (b and e) CO_2 conversion and CO selectivity and (c and f) hydrocarbon distribution. Reaction conditions: 40 bar, 6000 mL $g_{cat}^{-1}h^{-1}$ and H_2:CO_2 = 3:1 M ratio in the feed.

yield increases for the 3:1 mass ratio catalyst when compared with the 2:1 mass ratio due to the presence of a higher mass fraction of In_2O_3 catalyst (as mentioned earlier). The kinetic model predicts that the In_2O_3/HZSM-5 (3:1) catalyst shows slightly higher CO selectivity (specifically at the higher temperatures where RWGS reaction is more prominent) and CO_2 conversion (~10 % higher) when compared with the model predictions for the In_2O_3/HZSM-5 (2:1) catalyst (Fig. 8e). As mentioned earlier, the In_2O_3/HZSM-5 (3:1) catalyst produces more methanol since more In_2O_3 is present, but there is less zeolite to convert it. As a result, more methanol remains and this is not favorable for suppression of the RWGS reaction, hence increasing the CO concentration. This is especially the case at higher temperatures where the methanol synthesis is more strongly equilibrium limited. Both the experiments and model appear to predict these differences in CO_2 conversion and CO selectivity (Fig. 8b and e) between the different mass ratios of catalyst which strengthens the validity of the model.

From Fig. 8 (c and f), it can be seen that at temperatures below about 300 ℃, the model and experiments predict different distributions of C_2-C_4 vs C_5-C_8 hydrocarbons, however, these differences are small and for the experiments, they are more uncertain due to greater uncertainties of measurements at low conversion. On the other hand, at higher temperatures, the differences in the distributions are clearer and more consistent where both model and experiment for the 3:1 catalyst ratio show that the hydrocarbon distribution is shifted slightly more towards C_5-C_8 hydrocarbon products. Further, the calculation of the net reaction rates (shown in the SI, Table S5) for the formation of C_2-C_4 vs C_5-C_8 hydrocarbons and their relative differences support the distributions observed for the simulations shown in Fig. 8 (f). Also, from Table S5 it is observed that for almost all temperatures there is a slightly higher total rate of consumption of CH_3OH in the reactor with the 3:1 catalyst mass ratio, despite the fact that with this catalyst ratio there is less zeolite in the reactor. This is made possible due to the higher concentration of CH_3OH in the reactor with the 3:1 catalyst ratio. Apparently, a higher or near equal rate of consumption of CH_3OH over less zeolite favors the formation of a greater amount of higher hydrocarbons at higher reaction temperatures. Hence, we can conclude that increasing the supply of methanol to less zeolite apparently shifts the hydrocarbon product distribution to a slightly higher share of higher hydrocarbons.

Moreover, Fig. S10 shows a series of parity plots for the outlet mole fractions of methanol, C_2-C_4 and C_5-C_8 hydrocarbons comparing the simulated data with the experimental measurements. The parity plots showed good agreement between the experimental mole fractions of each of these species and those calculated by the model, thereby showing that this kinetic model predicts the data with good accuracy.

4. Conclusions

In this work, we have developed and demonstrated a kinetic model for the direct CO_2 hydrogenation to hydrocarbon over an In_2O_3/HZSM-5 bifunctional catalytic bed that combines two different models: an LHHW kinetic model for the CO_2 hydrogenation to methanol over the metal oxide In_2O_3 and a lumped type kinetic model for the conversion of methanol to hydrocarbons over the zeolite. Reaction rate constants, activation energies, adsorption equilibrium constants and enthalpies of adsorption along with their normalized sensitivity coefficients have been evaluated for the model. Experimental findings have been used to validate the model. This model allows prediction of the product distribution of the CO_2 hydrogenation reaction over the bifunctional catalytic bed performed when pure H_2 and CO_2 have been used as feeds. The key findings from the experiments and kinetic model for direct CO_2 hydrogenation to hydrocarbon can be summarized as follows:

a) The combined model for direct CO_2 hydrogenation to hydrocarbon over the bifunctional catalytic bed (In_2O_3/HZSM-5) could largely predict the experimental findings, such as the suppression of the RWGS reaction and increased yield of hydrocarbons compared to the formation of pure methanol with only the methanol synthesis catalyst (In_2O_3) under same reaction conditions.
b) The CO_2 to methanol kinetic model included the equilibrium effects on the methanol synthesis and RWGS reactions and this

demonstrates that the suppression of the RWGS reaction is primarily a favorable equilibrium effect resulting from the immediate conversion of the methanol by the MTH reactions to form hydrocarbons.

c) In addition, this understanding of how the alleviation of methanol synthesis equilibrium limitation suppresses the RWGS reaction was further validated by the experiments with varying weight ratios of the individual catalysts. Here it was seen that a higher outlet concentration of methanol achieved with a higher weight ratio of the methanol synthesis catalyst caused less suppression of the RWGS reaction. These conditions, which were slightly more favorable for the RWGS, also resulted in lower selectivity of hydrocarbons and a slightly increased share of higher hydrocarbons which were both also successfully reproduced by the model.

However, there may have been other interactions due to the combination of the catalysts that were unaccounted for by the model. For example, possible inhibiting effects of higher water concentration and hydrocarbons on the CO_2 to methanol catalyst (In_2O_3) and high concentrations of CO_2 and H_2 on the MTH catalyst (HZSM-5). These factors may deserve further investigation. This kinetic modeling study can also further be extended considering phenomena like the coke formation and catalyst deactivation that play a major role in this type of reaction.

Declaration of Competing Interest

The authors declare that they have no competing financial interests or personal relationships that could have appeared to influence the work reported in this paper

Acknowledgments

This work was performed at the Chemical Engineering division and the Competence Centre for Catalysis (KCK), Chalmers University of Technology and was conducted in collaboration with IVL Swedish Environmental Research Institute, Jämtkraft, Chemical Engineering at Lund University, Fly Green Fund och NISA, AFAB and The Power Region. We gratefully acknowledge the funding from the Swedish Energy Agency (47450-1 and 48387-1). Chalmers Materials Analysis Lab (CMAL) was used for most of the catalyst characterization. S.G. would like to acknowledge Dr. Joby Sebastian for helping with the different discussions on this work.

Appendix A. Supplementary data

Supplementary data to this article can be found online at https://doi.org/10.1016/j.cej.2022.135090.

References

[1] P. Gao, S. Li, X. Bu, S. Dang, Z. Liu, H. Wang, L. Zhong, M. Qiu, C. Yang, J. Cai, W. Wei, Y. Sun, Direct conversion of CO_2 into liquid fuels with high selectivity over a bifunctional catalyst, Nat. Chem. 9 (10) (2017) 1019–1024.

[2] Y. Wang, L.i. Tan, M. Tan, P. Zhang, Y. Fang, Y. Yoneyama, G. Yang, N. Tsubaki, Rationally Designing Bifunctional Catalysts as an Efficient Strategy To Boost CO_2 Hydrogenation Producing Value-Added Aromatics, ACS Catal. 9 (2) (2019) 895–901.

[3] Y. Xu, C. Shi, B. Liu, T. Wang, J. Zheng, W. Li, D. Liu, X. Liu, Selective production of aromatics from CO_2, Catal, Sci. Technol. 9 (3) (2019) 593–610.

[4] Z. He, M. Cui, Q. Qian, J. Zhang, H. Liu, B. Han, Synthesis of liquid fuel via direct hydrogenation of CO_2, Proc. Natl. Acad. Sci. U.S.A 116 (26) (2019) 12654–12659.

[5] M. Ronda-Lloret, G. Rothenberg, N.R. Shiju, A Critical Look at Direct Catalytic Hydrogenation of Carbon Dioxide to Olefins, ChemSusChem 12 (17) (2019) 3896–3914.

[6] P. Sharma, J. Sebastian, S. Ghosh, D. Creaser, L. Olsson, Recent advances in hydrogenation of CO_2 into hydrocarbons via methanol intermediate over heterogeneous catalysts, Catal. Sci. Technol. 11 (5) (2021) 1665–1697.

[7] D.A. Gunawardena, S.D. Fernando, Thermodynamic equilibrium analysis of methanol conversion to hydrocarbons using Cantera methodology, J. Thermodyn. 2012 (2012) 1–7.

[8] P. Tian, Y. Wei, M. Ye, Z. Liu, Methanol to olefins (MTO): From fundamentals to commercialization, ACS Catal. 5 (2015) 1922–1938.

[9] J. Sehested, Industrial and scientific directions of methanol catalyst development, J. Catal. 371 (2019) 368–375.

[10] E.L. Kunkes, F. Studt, F. Abild-Pedersen, R. Schlögl, M. Behrens, Hydrogenation of CO_2 to methanol and CO on $Cu/ZnO/Al_2O_3$: Is there a common intermediate or not? J. Catal. 328 (2015) 43–48.

[11] O. Martin, A.J. Martín, C. Mondelli, S. Mitchell, T.F. Segawa, R. Hauert, C. Drouilly, D. Curulla-Ferré, J. Pérez-Ramírez, Indium oxide as a superior catalyst for methanol synthesis by CO_2 hydrogenation, Angew. Chemie - Int. Ed. 55 (21) (2016) 6261–6265.

[12] S. Dang, B. Qin, Y. Yang, H. Wang, J. Cai, Y. Han, S. Li, P. Gao, Y. Sun, Rationally designed indium oxide catalysts for CO_2 hydrogenation to methanol with high activity and selectivity, Sci. Adv. 6 (2020) 1–11.

[13] J. Ye, C. Liu, D. Mei, Q. Ge, Active oxygen vacancy site for methanol synthesis from CO_2 hydrogenation on In_2O_3(110): A DFT study, ACS Catal. 3 (6) (2013) 1296–1306.

[14] I.M. Dahl, S. Kolboe, On the reaction mechanism for propene formation in the MTO reaction over SAPO-34, Catal. Letters. 20 (3-4) (1993) 329–336.

[15] I.M. Dahl, S. Kolboe, On the reaction mechanism for hydrocarbon formation from methanol over SAPO-34. I. Isotopic labeling studies of the co-reaction of ethene and methanol, J. Catal. 149 (2) (1994) 458–464.

[16] U. Olsbye, S. Svelle, M. Bjrgen, P. Beato, T.V.W. Janssens, F. Joensen, S. Bordiga, K. P. Lillerud, Conversion of methanol to hydrocarbons: How zeolite cavity and pore size controls product selectivity, Angew. Chemie - Int. Ed. 51 (2012) 5810–5831.

[17] I. Yarulina, A.D. Chowdhury, F. Meirer, B.M. Weckhuysen, J. Gascon, Recent trends and fundamental insights in the methanol-to-hydrocarbons process, Nat. Catal. 1 (6) (2018) 398–411.

[18] S. Ilias, A. Bhan, Mechanism of the catalytic conversion of methanol to hydrocarbons, ACS Catal. 3 (1) (2013) 18–31.

[19] R.A. Dagle, J.A. Lizarazo-Adarme, V. Lebarbier Dagle, M.J. Gray, J.F. White, D. L. King, D.R. Palo, Syngas conversion to gasoline-range hydrocarbons over $Pd/ZnO/Al_2O_3$ and ZSM-5 composite catalyst system, Fuel Process. Technol. 123 (2014) 65–74.

[20] F. Nestler, A.R. Schütze, M. Ouda, M.J. Hadrich, A. Schaadt, S. Bajohr, T. Kolb, Kinetic modelling of methanol synthesis over commercial catalysts: A critical assessment, Chem. Eng. J. 394 (2020), 124881.

[21] S. Ghosh, J. Sebastian, L. Olsson, D. Creaser, Experimental and kinetic modeling studies of methanol synthesis from CO_2 hydrogenation using In_2O_3 catalyst, Chem. Eng. J. 416 (2021), 129120.

[22] M.S. Frei, M. Capdevila-Cortada, R. García-Muelas, C. Mondelli, N. López, J. A. Stewart, D. Curulla Ferré, J. Pérez-Ramírez, Mechanism and microkinetics of methanol synthesis via CO_2 hydrogenation on indium oxide, J. Catal. 361 (2018) 313–321.

[23] G.H. Graaf, E.J. Stamhuis, A.A.C.M. Beenackers, Kinetics of low-pressure methanol synthesis, Chem. Eng. Sci. 43 (12) (1988) 3185–3195.

[24] X. Huang, D. Aihemaitijiang, W. De Xiao, Co-reaction of methanol and olefins on the high silicon HZSM-5 catalyst: A kinetic study, Chem. Eng. J. 286 (2016) 150–164.

[25] X. Huang, H. Li, W. De Xiao, D. Chen, Insight into the side reactions in methanol-to-olefin process over HZSM-5: A kinetic study, Chem. Eng. J. 299 (2016) 263–275.

[26] T.-Y. Park, G.F. Froment, Kinetic Modeling of the Methanol to Olefins Process. 1. Model Formulation, Ind. Eng. Chem. Res. 40 (20) (2001) 4172–4186.

[27] P. Kumar, J.W. Thybaut, S. Svelle, U. Olsbye, G.B. Marin, Single-event microkinetics for methanol to olefins on H-ZSM-5, Ind. Eng. Chem. Res. 52 (4) (2013) 1491–1507.

[28] A.T. Aguayo, D. Mier, A.G. Gayubo, M. Gamero, J. Bilbao, Kinetics of methanol transformation into hydrocarbons on a HZSM-5 zeolite catalyst at high temperature (400–550 °C), Ind. Eng. Chem. Res. 49 (24) (2010) 12371–12378.

[29] M. Kaarsholm, B. Rafii, F. Joensen, R. Cenni, J. Chaouki, G.S. Patience, Kinetic Modeling of Methanol-to-Olefin Reaction over ZSM-5 in Fluid Bed, Ind. Eng. Chem. Res. 49 (1) (2010) 29–38.

[30] P. Pérez-Uriarte, A. Ateka, A.T. Aguayo, A.G. Gayubo, J. Bilbao, Kinetic model for the reaction of DME to olefins over a HZSM-5 zeolite catalyst, Chem. Eng. J. 302 (2016) 801–810.

[31] T. Liang, J. Chen, Z. Qin, J. Li, P. Wang, S. Wang, G. Wang, M. Dong, W. Fan, J. Wang, Conversion of Methanol to Olefins over H-ZSM-5 Zeolite: Reaction Pathway Is Related to the Framework Aluminum Siting, ACS Catal. 6 (2016) 7311–7325.

[32] R. Gounder, E. Iglesia, Catalytic hydrogenation of alkenes on acidic zeolites: Mechanistic connections to monomolecular alkane dehydrogenation reactions, J. Catal. 277 (2011) 36–45.

[33] M.S. Frei, C. Mondelli, A. Cesarini, F. Krumeich, R. Hauert, J.A. Stewart, D. Curulla Ferré, J. Pérez-Ramírez, Role of Zirconia in Indium Oxide-Catalyzed CO_2 Hydrogenation to Methanol, ACS Catal. 10 (2) (2020) 1133–1145.